Journal of
Applied Crystallography
ISSN 1600-5767

Crystal chemistry of clinker relicts from aged cementitious materials

Michele Secco, Luca Peruzzo, Laurie Palasse, Gilberto Artioli, Alberto Viani and Alessandro Francesco Gualtieri

J. Appl. Cryst. (2014). **47**, 1626–1637

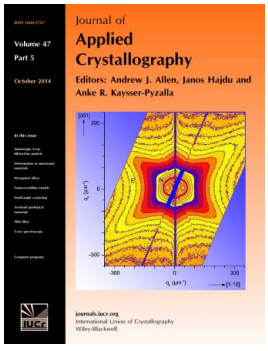

Many research topics in condensed matter research, materials science and the life sciences make use of crystallographic methods to study crystalline and non-crystalline matter with neutrons, X-rays and electrons. Articles published in the *Journal of Applied Crystallography* focus on these methods and their use in identifying structural and diffusion-controlled phase transformations, structure-property relationships, structural changes of defects, interfaces and surfaces, *etc.* Developments of instrumentation and crystallographic apparatus, theory and interpretation, numerical analysis and other related subjects are also covered. The journal is the primary place where crystallographic computer program information is published.

Journal of
Applied Crystallography
ISSN 1600-5767

Received 5 May 2014
Accepted 10 August 2014

Crystal chemistry of clinker relicts from aged cementitious materials

Michele Secco,[a,b]* Luca Peruzzo,[c] Laurie Palasse,[d] Gilberto Artioli,[a,e] Alberto Viani[f] and Alessandro Francesco Gualtieri[g]

[a]Inter-Departmental Centre for the Study of Cement Materials and Hydraulic Binders (CIRCe), University of Padua, Via Gradenigo 6, Padua 35131, Italy, [b]Department of Civil, Environmental and Architectural Engineering (ICEA), University of Padua, Via Marzolo 9, Padua 35131, Italy, [c]Institute of Geosciences and Georesources (IGG), National Research Council (CNR), Via Gradenigo 6, Padua 35131, Italy, [d]Bruker Nano GmbH, Bruker GmbH, Schwarzschildsrasse 12, Berlin 12489, Germany, [e]Department of Geosciences, University of Padua, Via Gradenigo 6, Padua 35131, Italy, [f]Centre of Excellence Telc, Institute of Theoretical and Applied Mechanics (ITAM), Batelovská 485-486, Telc 58856, Czech Republic, and [g]Department of Chemical and Geological Sciences, University of Modena and Reggio Emilia, Via S. Eufemia 19, Modena 41121, Italy. Correspondence e-mail: michele.secco@unipd.it

Despite the general tendency to consider Portland cement virtually fully hydrated within a few years, the occurrence of non-reacted clinker phases in cementitious materials that are several decades old is rather common. In this work, the integration of microstructural analysis by scanning electron microscopy and quantitative microchemical and micromineralogical characterization techniques, such as electron microprobe analysis and electron backscatter diffraction, allowed the definition of the crystal-chemical properties of partially hydrated cement residuals within different types of aged cementitious materials. The results on several clinker relicts show that the calcium silicate phases are transformed systematically and pervasively by hydration reactions, whereas the aluminate and ferrite phases do frequently persist in the anhydrous state. These relict phases may be distinguished through their peculiar chemical, mineralogical and textural features. These observations raise interesting questions concerning the long-term hydration kinetics of clinker phases and the durability behaviour of cementitious materials in operating conditions.

1. Introduction

Understanding the mechanisms of cement hydration has been one of the major goals of materials scientists since the first Chemistry of Cement Conference one hundred years ago. Nowadays, after one century of theoretical and experimental studies, remarkable progress has been made in the characterization and modelling of the chemical–physical processes responsible for the setting and hardening of cement-based materials (Bullard *et al.*, 2011; Gaidis & Gartner, 1989; Gartner & Gaidis, 1989; Gartner *et al.*, 2002; Scrivener & Nonat, 2011; Taylor *et al.*, 1984). Yet, several open questions, especially concerning the details of theoretical models, stimulate the continuing efforts of the scientific community to understand fully the mechanisms acting during hydration of the cement system.

The reaction kinetics of the clinker phases are certainly one of the issues that are most actively investigated, both from the experimental (Asaga *et al.*, 1992; Gutteridge & Dalziel, 1990; Hoshino *et al.*, 2006; Kocaba, 2010; Merlini *et al.*, 2008; Taylor, 1997; Schlegel *et al.*, 2012) and from the modelling (Bishnoi & Scrivener, 2009; Bullard, 2008; Garrault *et al.*, 2010; Lothenbach & Winnefeld, 2006) points of view. Abundant data are available on the dissolution and the surface reactivity of each clinker phase over time. Literature data agree in indicating tricalcium silicate (C_3S in cement chemistry notation, also identified with the name of its stable polymorph alite) and tricalcium aluminate (C_3A in cement chemistry notation, abbreviated as aluminate) as the most reactive phases in the Portland system, showing degrees of reaction at one day of hydration of about 40–60% for alite and 20–80% for aluminate (Kocaba, 2010; Taylor, 1997). Dicalcium silicate (C_2S in cement chemistry notation, also identified with the name of its stable polymorph belite) has slower reaction kinetics at early ages with respect to the other phases, with degrees of reaction lower than 20% at seven–ten days (Kocaba, 2010; Taylor, 1997). This is mainly due to slower dissolution caused by the ion concentrations in the solution produced by alite, which has higher solubility (Scrivener & Nonat, 2011). Nevertheless, the delayed hydration of belite is fundamental for the long-term strength development of cementitious materials.

In the same way as aluminate, the reaction kinetics of tetracalcium aluminoferrite (C_4AF in cement chemistry notation, abbreviated as ferrite) are universally considered to be very fast during the early hydration stages, though the

hydration progression at later ages is cause for controversy. Some authors hypothesize an interruption of the reaction process, possibly due to the formation of a passivating layer of iron hydroxides on the crystals (Taylor, 1997), whereas others claim an almost total hydration of these phases (Kocaba, 2010).

The discrepancy between different and equally reliable observations possibly stems from the fact that most studies of cement hydration have been carried out using severe simplifications:

(i) Experimental data on reaction kinetics are generally obtained for simplified chemical systems constituted by pure phases, generally disregarding the substantial isomorphic substitutions and polymorphic transformations affecting the crystal-chemical nature and reactivity of the clinker phases in real systems, as proved by several studies (Taylor, 1997; Costoya, 2008; Garrault & Nonat, 2001).

(ii) Experiments frequently rely on simplified mixtures with a reduced number of components (*e.g.* C_3A-gypsum, C_3S, C_3A-gypsum; Favero, 2013; Quennoz & Scrivener, 2012) to minimize the cross-correlation effects between the various parameters in the reaction processes. This obviously has the advantage of isolating specific mechanisms, although it is a severe simplification over real systems, which clearly experience domino effects between the reactions acting at the same time.

(iii) In the investigation of the hydration kinetics of simplified cementitious systems, the effects of nominally inert and/or partially reactive phases are seldom taken into account, though they are invariably present in real conglomeratic materials containing aggregates (mortars, plasters, concretes).

(iv) The crystal-chemical features of residual anhydrous phases and the reaction progression at long hydration ages in real systems are rarely taken into account.

Despite the shortage of extensive and specific crystal-chemical characterization at long maturation times, cement is commonly considered virtually fully hydrated within a few years (Taylor, 1997). This is clearly at variance with several studies pointing out the presence of unreacted clinker phases (mainly belite and ferrite) in concretes that are decades old, and sometimes even intensely altered (Gebauer & Harnik, 1975; Hearn *et al.*, 1994; Scrivener & Nonat, 2011; Taylor *et al.*, 2010; Gao, 1999). As far as the specific presence of the ferrite phase is concerned, its occurrence is generally justified in the literature by invoking incongruent dissolution of the phase. The mechanism assumes the almost pseudomorphic replacement of the ferrite interstitial phase by iron oxides and hydroxides, whereas the calcium and alumina components migrate and are included into the hydration products (Scrivener & Nonat, 2011). However, almost no detailed microstructural, chemical and mineralogical investigations are available concerning the nature and characteristics of these hydration relicts. This is probably due to the difficulty in performing reliable and quantitative chemical–mineralogical analyses of such heterogeneous, microcrystalline and possibly nonstoichiometric compounds (Taylor, 1997). A clear example of the issues related to the problematic analysis of such clinker relicts using routine approaches is reported in Fig. 1(*a*), where a clinker particle in a 50-year-old concrete sample has been imaged and analysed by means of scanning electron microscopy (SEM) with an associated energy-dispersive X-ray spectroscopy (EDS) system. The obtained backscattered electron (BSE) image (BEI) shows the presence of calcium silicate phases that seem to be widely reacted, while the interstitial phase is apparently still anhydrous. The EDS analysis of the area characterized by higher BSE signal (blue square in the image) suggests a chemical composition compatible with a ferrite phase with significant isomorphic substitutions, although the lack of quantitative chemical data and crystallographic information does not allow a clear identification of the mineral phase(s). In this case X-ray powder diffraction analyses were inconclusive because of the presence of numerous diffraction peaks due to the aggregate phases and the hydration products, which almost totally obliterate the diffraction signal of the relict phases (Fig. 1*b*), even after thorough separation of the grain fraction under 40 µm from the conglomerate.

Within this frame, only the adoption of a combined analytical approach encompassing both standard microstructural analysis by SEM-EDS and advanced methodologies for

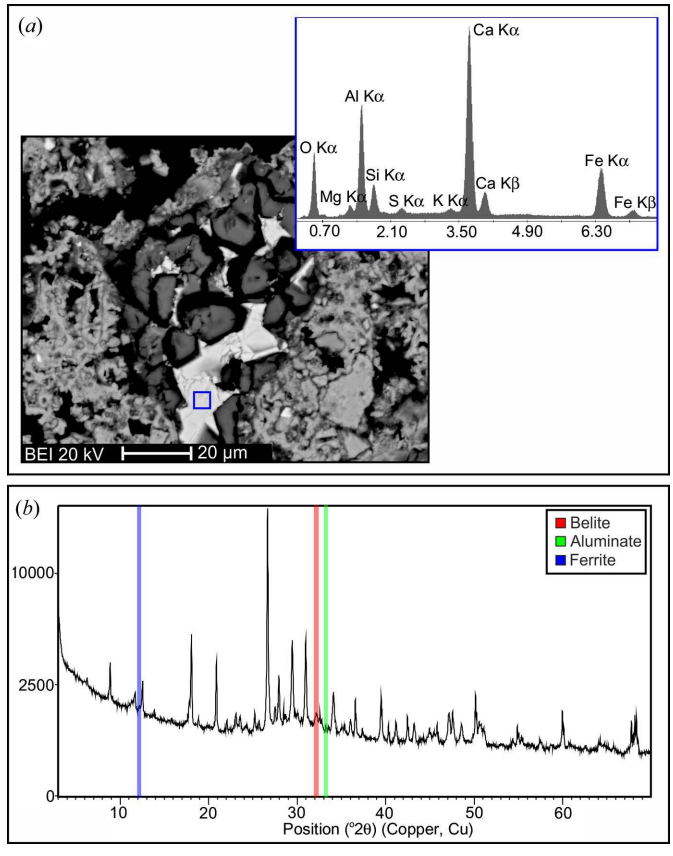

Figure 1
(*a*) Example of SEM-EDS microanalysis on a clinker relict from a 50-year-old concrete sample (a BEI and EDS microanalysis from an interstitial phase portion are reported). (*b*) X-ray powder diffraction pattern of the same concrete sample (fraction < 40 µm). The angular positions of the more intense diffraction peaks of relict clinker phases are highlighted.

compositional and mineralogical characterization under the micrometre scale seems to be suitable to overcome the experimental difficulties. Electron microprobe analysis (EMP) coupled with a wavelength-dispersive X-ray spectroscopy (WDS) system and electron backscatter diffraction (EBSD) are potentially suitable to quantitatively integrate the results obtained by SEM-EDS at the microscale. Specifically, EMP-WDS yields an accurate quantitative measurement of the elemental composition of any compound, both crystalline and amorphous, allowing precise stoichiometric calculations. The EBSD technique, based on electron diffraction produced by the crystal lattice, turns out to be fundamental to reveal the crystalline nature of the analysed compound at the sub-micrometre scale and to identify the crystal phase. The data on the crystal orientation acquired by EBSD also provide further information for microtextural interpretation. EBSD has been widely applied in recent years in many different fields such as metallurgy, materials sciences, mineralogy, earth sciences and archaeometry (Adams *et al.*, 1993; Peruzzo *et al.*, 2011; Prior *et al.*, 1999; Lloyd, 1987; Schwartz *et al.*, 2009; Wilkinson & Hirsch, 1997). Following a preliminary study on asbestos cement (Viani *et al.*, 2013), to our knowledge this represents the first case in which EBSD is systematically applied in the field of cementitious materials.

2. Experimental procedure

2.1. Materials and sample preparation

Eight samples were selected for the investigation, representing different types of cementitious materials, namely concrete structural elements (four samples), asbestos cement manufactured products (three samples) and a steel fibre reinforced cement flooring (one sample). A brief description of each sample follows:

(i) TCR: a portion of a structural reinforced concrete beam from the Victory Monument (Bolzano, northeastern Italy), built in 1928. Despite the age, the chemical and mineralogical characteristics of the binder utilized for the manufacturing of the structural element are similar to modern Portland cements (Secco, 2012), clearly indicating a rotary kiln production of the clinker. The material was sampled with a metal chisel from a widely altered external portion of the structural element, with significant progression of the carbonation phenomena, oxidation of the rebars and occurrence of alkaline sulfate crystallization.

(ii) BS1: a portion of a structural non-reinforced cyclopic concrete wall from the same building as the TCR sample. The characteristics of the binder are similar to those of the previous sample, and the material was sampled from an internal, unperturbed portion of a core extracted with a water-lubricated diamond coring system. The material does not show signs of macroscopic alteration.

(iii) VR-P1: a portion of a structural reinforced concrete column from the automated refrigeration plant of the Magazzini Generali complex (Verona, northeastern Italy), built in 1928. Also in this case, the binder has chemical–mineralogical characteristics similar to modern Portland cements, indicating a rotary kiln production (Secco, 2012). The material was sampled with a metal chisel from an altered external portion of the structural element, distinguished by significant percolation of meteoric water.

(iv) P3E: a portion of a structural reinforced concrete column of the old Foro Boario in Padua (northeastern Italy), built in 1968. A binder classifiable as CEM I-type cement (European Standard EN 197-1) was used. The material was sampled by dry removal of a superficial portion of the element with a hammer drill. The sample was found to be totally unaltered (Secco, 2012).

(v) CA9, CA12, CA14: asbestos cement samples taken by mechanical removal from different types of manufactured products (a corrugated slab, a board and a pipe, respectively). The materials are all of Italian production, and they were manufactured between the 1960s and the 1980s. Amongst the three analysed samples, CA12 and CA14 have been produced with binders classifiable as CEM I-type cements, whereas a binder classifiable as a CEM III slag cement was used for CA9 (Viani *et al.*, 2013). As regards the conservation state, CA12 and CA14 show little or no alteration, while CA9 is significantly carbonated (Viani *et al.*, 2013).

(vi) PS1: a portion of steel fibre reinforced cementitious flooring, manufactured in the 1980s with a binder classifiable as a CEM I-type cement and steel flakes as aggregate. The material was sampled with a metal chisel from a widely altered superficial portion, distinguished by significant carbonation and external sulfate attack phenomena.

In order to preserve the sampled materials in the pristine state, the preparation procedures were performed avoiding all possible interactions between water fluids and exposed surfaces. First, the analysed materials were stabilized by embedding them in epoxy resin, operating under vacuum to facilitate impregnation. Transverse sections were then exposed by dry cutting. The concrete samples were thin sectioned, while a direct preparation of the exposed surfaces was performed on the other samples. The materials were preliminarily lapped in order to operate a first removal of the deformation layer introduced during sectioning and to obtain a flat surface for examination. Lapping was performed in a three-step procedure: (i) lapping until planar using a 220 grit SiC paper; (ii) manual lapping for 20 s using a 500 grit SiC powder; (iii) manual lapping for 20 s using a 800 grit SiC powder. The materials were then cleaned in an ultrasonic bath, subjected to three cycles of preliminary polishing of 20 s each with a 1200 grit SiC powder, and again cleaned in an ultrasonic bath. All the lapping and pre-polishing procedures were carried out using ethylene glycol as liquid medium, while the cleaning procedures were performed employing ethanol. Then, the samples were subjected to an accurate polishing procedure with an automatic polishing machine in order to remove any deformation introduced during lapping. Polishing was performed in a two-step procedure: (i) preliminary polishing on a silk cloth for 5 min with a 6 μm alcohol-based diamond solution; (ii) final polishing on a silk cloth for 5 min with a 1 μm alcohol-based diamond solution. The specimens

were then accurately polished by means of a vibratory polisher with colloidal silica for 30 min, cleaned with ethanol and finally coated with a layer of carbon, thin enough to allow the EBSD pattern from the sample to be detected and acquired, but thick enough to avoid charging effects on the sample's surface.

2.2. Analytical methods

2.2.1. SEM-EDS. A CamScan MX2500 scanning electron microscope was used, equipped with an LaB_6 cathode and a four-quadrant solid-state BSE detector for imaging. The analytical conditions were as follows: accelerating voltage: 20 kV; filament current: 1.80 A; emission current: 20 μA; aperture current: 300 nA; working distance: 20–30 mm. For microanalysis and X-ray mapping, an EDAX-EDS energy dispersive X-ray fluorescence spectrometer was used, equipped with a Sapphire detector composed of a LEAP+ Si(Li) crystal and a super ultra thin window.

For each sample, in order to choose the most representative portions to be analysed, a first BSE observation allowed evident compositional zoning or variations to be detected. Subsequently, spot microanalyses allowed the elemental composition to be estimated (by the *SEM Quant/Phizaf* software; Goldstein *et al.*, 1992).

On the basis of this preliminary analysis, several X-ray maps were collected at about 10–15 $\times$ 10^3 counts per second using the automated EDX-imaging/mapping software (Goldstein *et al.*, 1992) at different conditions, depending on the size of the detail to be examined. Maps of 512 $\times$ 400 pixels with 200 ms dwell time were acquired simultaneously for Fe, Ca, Si, Al, Na, K, Mg, S and Ti, assigning a different colour to each element. An auto scaling function was then applied so that each resulting map showed the relative variation in the amount of each element in the scanned region, where the lower colour intensity corresponds to the lower content of that element measured in the whole area. Finally, the superimposition of individual maps of selected elements produced one combined map in which different colours, representing different compositional ranges, can be directly assigned to specific mineral phases.

The well known limit for this kind of semi-quantitative analysis is related to the insensitivity to light elements, such as hydrogen in water (both structural and adsorbed) and hydroxyl groups. Thus, quantitative EMP-WDS analysis was adopted in order to chemically discriminate between hydrated and anhydrous phases in the analysed materials.

2.2.2. EMP-WDS. Homogeneous grains or areas identified by SEM as possible mineral phases of clinker relicts were analysed by electron microprobe to get an absolute assessment of their chemical composition.

The instrument used was a Cameca SX50 equipped with four wavelength-dispersive spectrometers, at the CNR-IGG laboratory in Padua. Typical measurement conditions were 20 kV acceleration potential, 20 nA beam current, 10 s acquisition time on peak and 5 s on background positions. The following standards were used for calibration of specific chemical elements: periclase (Mg); ilmenite (Mn, Ti); diopside (Ca, Si); corundum (Al); hematite (Fe); orthoclase (K); albite (Na). The *Cameca-PAP* program (Pouchou & Pichoir, 1985) was used to convert X-ray counts into oxide weight percentages. Analyses are accurate within 2% relative for major and 5% relative for minor elements.

Owing to the small size of the targets (commonly around 10 μm or less) and the tight intergrowth of the different phases, many consecutive spot analyses were run very close together. Subsequently, only those analyses unaffected by boundary and mixed-phase effects were selected. Combining this screening strategy with stoichiometric calculations, we obtained measurements showing oxide sums close to 100%, which are a good indication that the related phases are anhydrous.

2.2.3. EBSD. To investigate the possible permanence of a crystalline residual fraction of non-reacted clinker phases from the cements used for the production of the analysed materials, micromineralogical analyses on selected samples were performed by means of the EBSD technique.

The ESBD technique is based on the principle that a crystalline phase can diffract the primary electrons of a scanning electron microscope beam, producing a pattern (namely an EBSP) recordable by a suitable detector. The diffraction pattern can be used to determine crystal orientations and of course to discriminate between different materials, as shown in this case. Phase identification obtainable through EBSD is often impossible to obtain by other methods such as X-ray diffraction, WDS, transmission electron microscopy and so on, as (i) the particles are too small; (ii) the particles are too few; (iii) the particles are intrinsically dispersed in a complex texture and do not provide a recognizable signal, or they cannot be separated and concentrated; and (iv) their chemistry does not allow discrimination between different minerals having similar composition. Such limitations can frequently be overcome by using the EBSD technique because the diffraction signal is produced by particles smaller than 1 μm, which can be appropriately observed and identified by SEM–BSE imaging.

The EBSD analyses were performed at the Department of Geosciences (University of Padua) using an LaB_6 Camscan MX2500 scanning electron microscope, equipped with a Nordif CCD camera, an Argus 20 (Hamamatsu) image processor and the *CHANNEL 5* software (HKL Technology, Hobro, Denmark) to detect and process the EBSD signal. The analytical conditions were as follows: accelerating voltage: 30 kV; filament emission: 160 mA; working distance: 25 mm; stage tilting: 70°.

The following structural models of the main clinker phases were used for the creation of the reference EBSD reflector data: alite M3 (Nishi *et al.*, 1985), belite β (Mumme *et al.*, 1995), cubic aluminate (Wong-Ng *et al.*, 1987), orthorhombic aluminate (Nishi & Takeuchi, 1975), ferrite (Colville & Geller, 1972).

Additional analyses were performed on two selected samples (CA9, CA12) at the Bruker Nano laboratory, where EDS X-ray maps were acquired simultaneously with EBSD in

order to check the effective coincidence of the area compositional distribution and the corresponding diffraction patterns.

The EBSD analyses were performed using a Bruker QUANTAX CrystAlign EBSD analysis system mounted on a Tescan VEGA3 XM scanning electron microscope, equipped with an e-Flash 1000 camera, an ARGUS forescattered/backscattered electron imaging system and the *ESPRIT* software (Goldstein *et al.*, 1992) to detect and process the EBSD signal. The simultaneous EDS analyses were performed using a Bruker XFlash 5030 silicon drift detector. The analytical conditions were as follows: accelerating voltage: 30 kV; filament emission: 160 mA; working distance: 17 mm; stage tilting: 70°.

3. Results

3.1. SEM-EDS

The preliminary analyses of the materials by means of BSE imaging (Fig. 2) highlighted the systematic presence of relict particles characterized by dimensions of between 20 and 150 µm, irregular shapes, and high backscattered electron signal (white in the pictures). They are uniformly dispersed in the cementitious matrices and their total amount is variable, from moderate (Fig. 2*a*) to extremely high (Fig. 2*d*), with no evident correlation with the type of cementitious material, binder typology and alteration state.

At greater magnification, it is possible to observe peculiar morphologies of the clinker relicts (Fig. 3), which maintain at times the pristine shape of the anhydrous grain despite a significant and heterogeneous reaction of the anhydrous phases (Figs. 3*a*, 3*d*, 3*e* and 3*f*), whereas in other cases they show a high degree of reaction but less defined morphology (Figs. 3*b* and 3*c*).

A common characteristic of all relict particles is the presence of a dense skeleton with high BSE signal, apparently composed of largely or totally nonreacted interstitial phases. The skeleton encloses less dense areas with euhedral to subhedral morphology (labelled as C in Figs. 3 and 5), having lower BSE signal, indicating a significantly lower mean atomic number with respect to the main constituents of the skeletal structure.

The skeletal microstructure shows chemical heterogeneities at micrometre scale [indicated by different intensities in the backscattered electron emission, with portions appearing slightly lighter than the others (labelled as F in Figs. 3, 5 and 6)], due to the presence of heavier atoms. Accordingly, the morphological features of the constituent phases are quite heterogeneous. The different compounds in some cases are clearly separated, with large homogeneous microstructural domains suggesting regular growth of single crystals (Fig. 3*b*), whereas in other cases it is possible to observe a more complex intergrowth of smaller crystals (Fig. 3*d*), and in extreme cases complex dendritic structures are present. On the basis of the point chemical analyses, the interstitial phase seems to be in most cases totally anhydrous; it shows virtually no porosity and the absence of clear reaction regions. In some cases, small etch pits are visible in the interfacial and external portions (Fig. 3*b*), suggesting limited phenomena of dissolution along

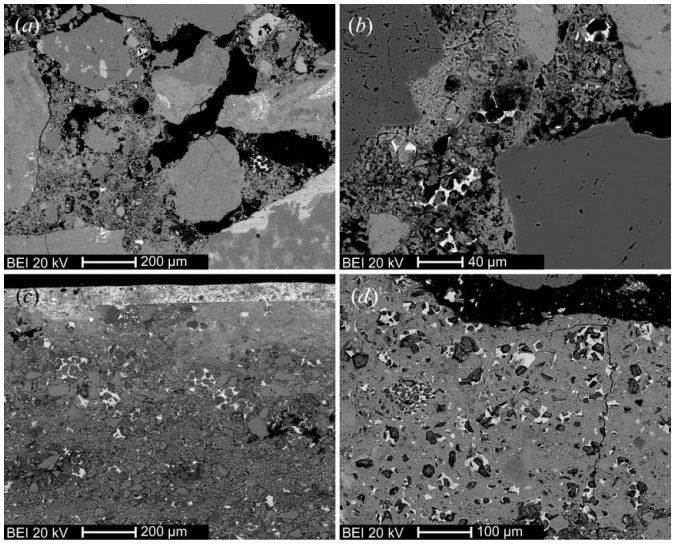

Figure 2
Selected low-magnification BEIs of four analysed samples. (*a*) TCR; (*b*) P3E; (*c*) CA12; (*d*) PS1.

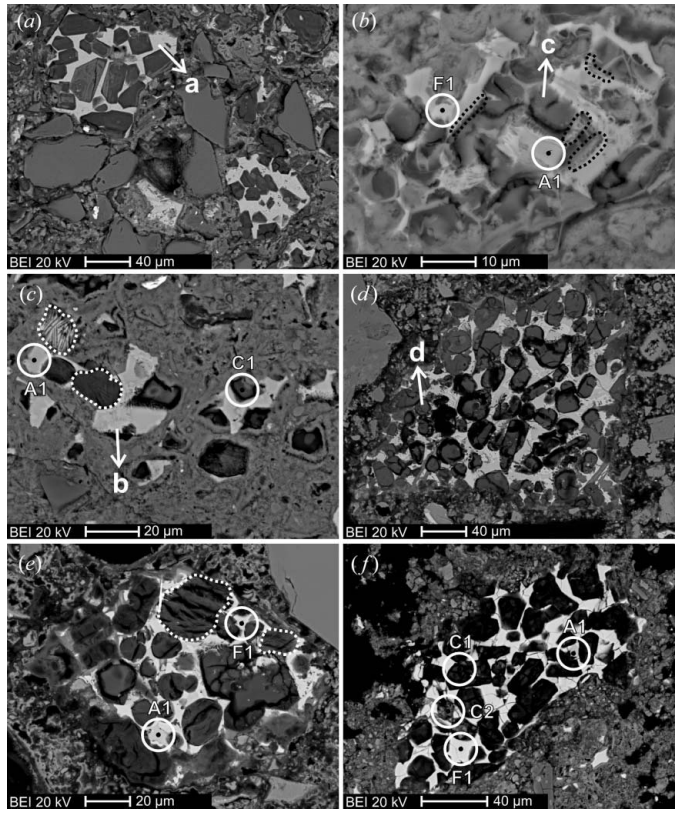

Figure 3
BEIs of several analysed clinker relicts. (*a*) CA12; (*b*) CA9; (*c*) PS1; (*d*) TCR; (*e*) BS1; (*f*) VR-P1. Arrow tips indicate the points of the SEM-EDS microanalyses reported in Fig. 4; circles indicate the points of the EMP-WDS analyses reported in Tables S1–S3; black dotted lines highlight etch pits caused by partial dissolution of interstitial phase constituents; white dotted lines highlight reacted calcium silicate grains showing internal microcracks arranged according to defined paths.

preferred paths, maybe triggered by the local presence of crystallographic defects (Juilland *et al.*, 2010).

The compositional heterogeneity was confirmed by EDS microanalyses on the skeletal structures, the darker portions being constituted mainly by calcium and aluminium plus minor amounts of iron, silicon, alkalis and magnesium (Fig. 4*a*), with an overall chemical composition very close to that of aluminate. The lighter portions are mainly constituted by calcium, aluminium and iron plus minor amounts of silicon and magnesium and traces of manganese and alkalis (Fig. 4*b*), with an overall chemical composition close to that of ferrite. The EDS microanalyses clearly point to the presence of aluminate and ferrite phases characterized by relevant chemical substitutions, with little sign of hydration reactions.

As far as the idiomorphic grains enclosed by the skeletal structures are concerned, several heterogeneities are observable. First of all, some grains have marked pseudo-hexagonal euhedral shapes, with the presence of sharp and clear angles (Figs. 3*a* and 3*f*), while others are subhedral, with less defined angles and, at times, rounded shapes (Figs. 3*d* and 3*e*). These features are typically used in cement petrography to discriminate alite from belite (St John *et al.*, 1998). Besides crystal habits, these microstructural sites are characterized by different textures of the constituent materials. In most cases they are almost completely filled by compounds having low BSE signal, indicating a significantly smaller mean atomic number with respect to the constituents of the skeletal structure.

It is also possible to observe small chemical heterogeneities, highlighted by different intensities of the BSE signal (Figs. 3*a* and 3*c*), while other samples show a greater degree of homogeneity (Figs. 3*b* and 3*d*). Despite the high degree of filling, a limited porosity is present, commonly in the form of microcracks arranged in the interfacial portions with the skeletal structure and distributed in the internal areas of the grains, both with random orientations (Figs. 3*b* and 3*d*) and according to defined paths (Figs. 3*c* and 3*e*) which suggest preferred reaction phenomena along striations formed because of crystal twinning (Scrivener, 2004).

In other cases, an overall lower density is observable in the grains, with higher porosity and only partial filling by solid compounds (Figs. 3*c* and 3*d*). Sometimes the grains are almost totally empty (Figs. 3*d* and 3*f*).

As shown by EDS microanalyses, the enclosed dark-grey areas are mainly constituted by calcium and silicon with minor amounts of aluminium, iron and magnesium and traces of alkalis and sulfur. The chemical composition is significantly heterogeneous, in particular as regards the relative amounts of calcium and silicon: the chemistry is variable despite being generally similar to that of the surrounding hydrated matrix (Fig. 4*c*). In specific regions the composition is significantly enriched in silicon (Fig. 4*d*), typical of heavily decalcified cementitious matrices.

Taking into account the observed features of the grains enclosed by the skeletal structures, it is possible to hypothesize relevant reaction phenomena of the calcium silicate phases,

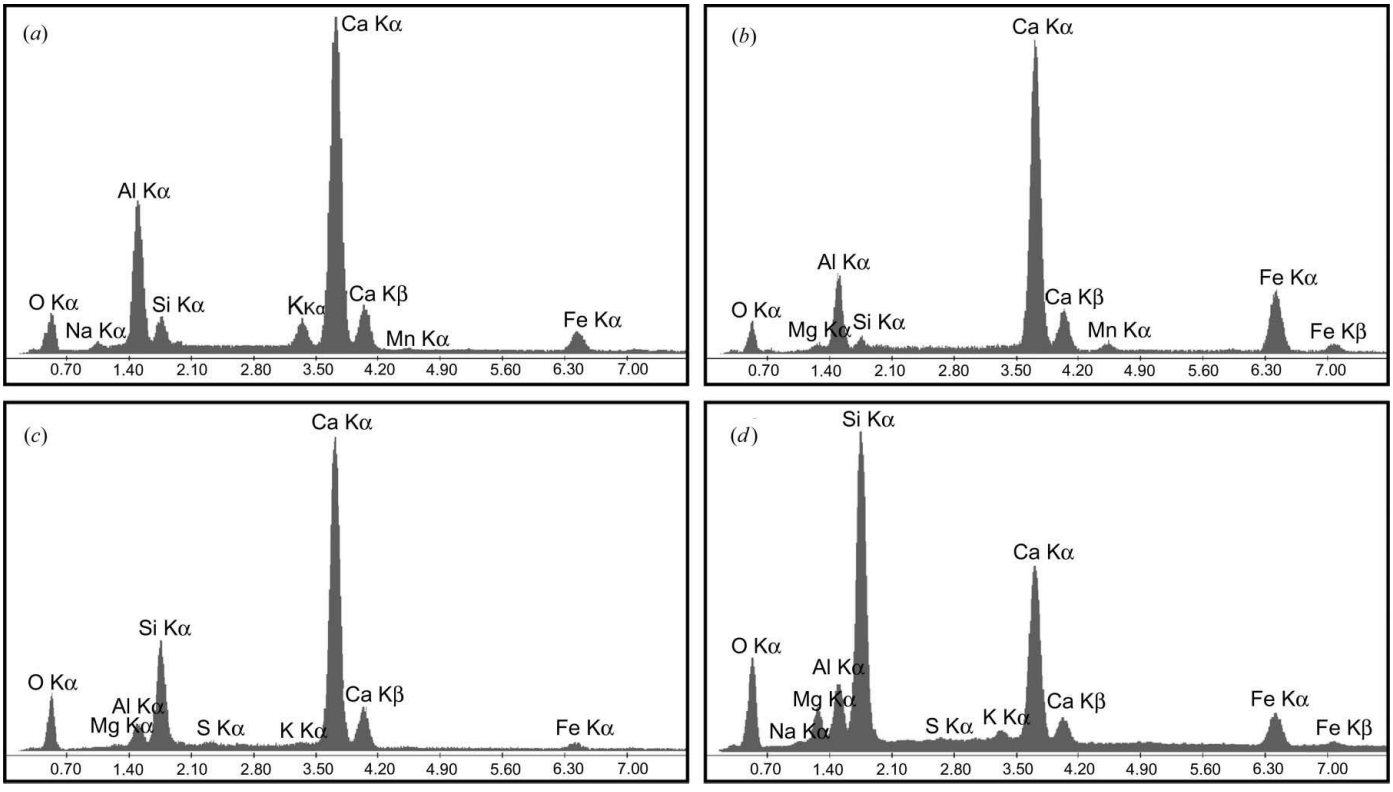

Figure 4
SEM-EDS microanalyses of the points indicated by arrows in Fig. 3.

with a prevailing pseudomorphic replacement of hydration products after alite and belite.

The features observed by SEM-EDS analysis are confirmed by chemical mappings performed on selected relicts. Four representative examples are reported in Figs. 5 and 6. (i) Relicts in the TCR and CA12 samples that retained the original shape of the particles (Fig. 5), showing a high degree of reaction of the calcium silicates (the grains are largely empty, at times partially or totally filled by Si-rich hydrated phases) and the almost total permanence in the anhydrous state of the interstitial phase, arranged in large and well defined crystal domains. (ii) Relicts in the P3E and CA14 samples (Fig. 6), showing a more subrounded shape of the original particles, a high degree of reaction of the calcium silicates (the grains are partially or totally filled by Si-rich hydrated phases) and the rather limited hydration of the interstitial phase (only a few etch pits are observable). Aluminate and ferrite are well discriminated in the smaller relict of the P3E sample (Fig. 6*a*), while a more chaotic intergrowth is observable in the largest one and in the relicts of the CA14 sample (Fig. 6*c*).

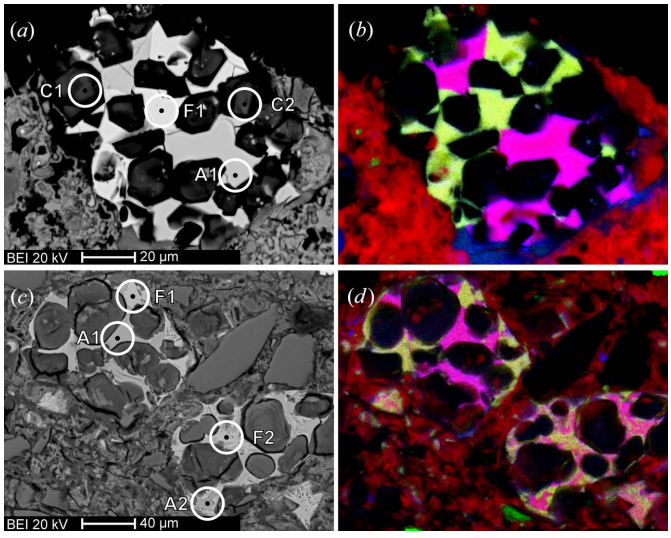

Figure 5
BEIs of clinker relicts in the TCR (*a*) and CA12 (*c*) samples, respectively, and EDS chemical maps of the same areas (*b*), (*d*), obtained by RGB merging of calcium, iron and aluminium elemental maps in the R, G and B bands, respectively. Circles indicate the points of the EMP-WDS analyses reported in Tables S1–S3.

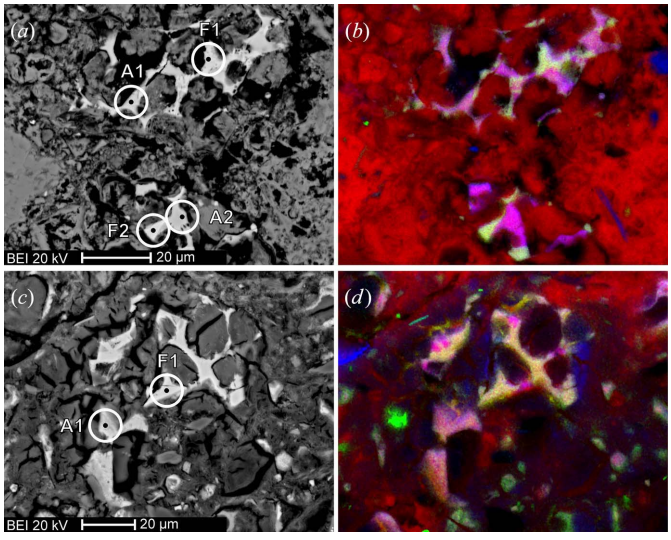

Figure 6
BEIs of clinker relicts in the P3E (*a*) and CA14 (*c*) samples, respectively, and EDS chemical maps of the same areas (*b*), (*d*), obtained by RGB merging of calcium, iron and aluminium elemental maps in the R, G and B bands, respectively. Circles indicate the points of the EMP-WDS analyses reported in Tables S1–S3.

3.2. EMP-WDS

A series of selected point analyses, acquired from areas unaffected by phase boundary effects up to the micrometre scale and identified as composed of aluminate and ferrite crystals by SEM-EDS analyses, are reported in Tables S1 and S2[1] of the supporting information, respectively, together with three reference average compositions for crystal phases in ordinary production clinkers, based on the results of several studies by X-ray microanalysis (Boikova *et al.*, 1980; Ghose & Barnes, 1979; Harrisson *et al.*, 1985; Kristmann, 1978; Sarkar & Roy, 1984). Several point analyses reported in the tables are marked in Figs. 3, 5 and 6 by circles. Weight percentages of the recalculated oxides are reported in the upper part of the tables, together with the total sum of oxides and the sum of alkali concentrations (Tables S1), commonly used in the literature to chemically discriminate between the cubic and the orthorhombic structures of aluminate (Takéuchi *et al.*, 1980). Calculated atomic ratios, normalized to six and five oxygen atoms for aluminate and ferrite, respectively, are reported in the lower part of the tables, together with the total sum of the cations partitioned between tetrahedral and octahedral sites, as suggested by Taylor (1997) (aluminate: aluminium, iron and silicon in the tetrahedral site, calcium, sodium, potassium, magnesium, manganese and titanium in the octahedral site; ferrite: aluminium, iron, silicon, magnesium, manganese and titanium in the tetrahedral site, calcium, sodium and potassium in the octahedral site). Pure C_3A and C_4AF compositions are totally absent; instead the analysed phases show a substantial degree of chemical substitution.

Furthermore, the overall sum of recalculated oxides is very close to 100% for all the point analyses performed. Accordingly, test measurements performed on several samples did not detect the occurrence of other measurable atomic species (*i.e.* sulfur and chromium) within the limit of detection. This experimental evidence points to the absence of hydrated phases in the microstructural skeleton sites occupied by interstitial phases, confirming the hypothesis that the aluminate and the ferrite phases in the analysed relicts are anhydrous.

The microanalyses detected clear chemical differences between the darker and the lighter portions of the skeletal structures visible in the backscatter electron imaging (Fig. 3).

[1] Supporting information for this article is available from the IUCr electronic archives (Reference: KS5433).

The former have generally high amounts of aluminium, with homogeneous mean values around 30 wt% of Al_2O_3. The CA12, CA14 and PS1 samples show slightly lower values. The aluminium concentrations in the lighter portions are more scattered but systematically lower with respect to the adjacent darker regions.

An inverse correlation is thus observable between the aluminium and the iron concentrations. The lighter regions show higher Fe_2O_3 values (mean 20 wt%) and they are interpreted as ferrite, whereas the darker regions show lower values (mean 10 wt%) and they are interpreted as aluminate (Fig. 7*a*). Further direct correlations are observable between (i) aluminium, calcium and alkali ions (darker portions) and (ii) iron, titanium and manganese (lighter portions), which point to incorporation of alkali into aluminate and of Ti and Mn into ferrite (Fig. 7*b*). Taking into account the total amount of alkali as a possible indicator of the structural modifications of the aluminate phases (Boikova *et al.*, 1977), samples BS1, P3E, CA9, CA14 and PS1 have values typical for cubic structures, and samples VR-P1 and CA12 for orthorhombic ones, while sample TCR is characterized by border values.

Concerning the cation partitioning between the crystallographic sites of the phases, it is possible to observe that, following the adopted model, the tetrahedral sites of both aluminate and ferrite always show an overall sum of ions close to the theoretical value of 2 expected by the crystal-chemical formula, with deviations included in the ±0.10 interval (Figs. 7*c* and 7*d*). In the octahedral sites, a good correspondence between the experimental sum of ions and the theoretical values of 2 (ferrite) and 3 (aluminate) is still observable, with deviations generally included in the ±0.12 interval (Figs. 7*c* and 7*d*). The larger deviations resulting from the analyses of the aluminate portions of the VR-P1 and CA9 samples, with values included in the ±0.22 interval, suggest the occurrence of substantial vacancy defects in the analysed material.

A series of selected point analyses from the dark-grey grains enclosed by the skeletal structures are reported in Tables S3 of the supporting information. The acquisition of reliable data was extremely difficult because of the low density and high internal porosity of the materials.

All point analyses acquired in these areas are characterized by low total sums of recalculated oxides, indicating both a relevant presence of light elements, such as hydrogen, and the occurrence of diffuse nanoporosity, not observable by EMP-WDS analyses. However, in agreement with the results of previous semi-quantitative SEM-EDS analysis, the EMP measurements clearly indicate that the material in the grains is mainly constituted by calcium and silicon, with extremely variable Ca/Si ratios, mostly between 1 and 2.5 but in several cases well below 1, the latter assumed to be consistent with heavily decalcified cementitious matrices. The experimental evidence strengthens the hypothesis of calcium silicate reac-

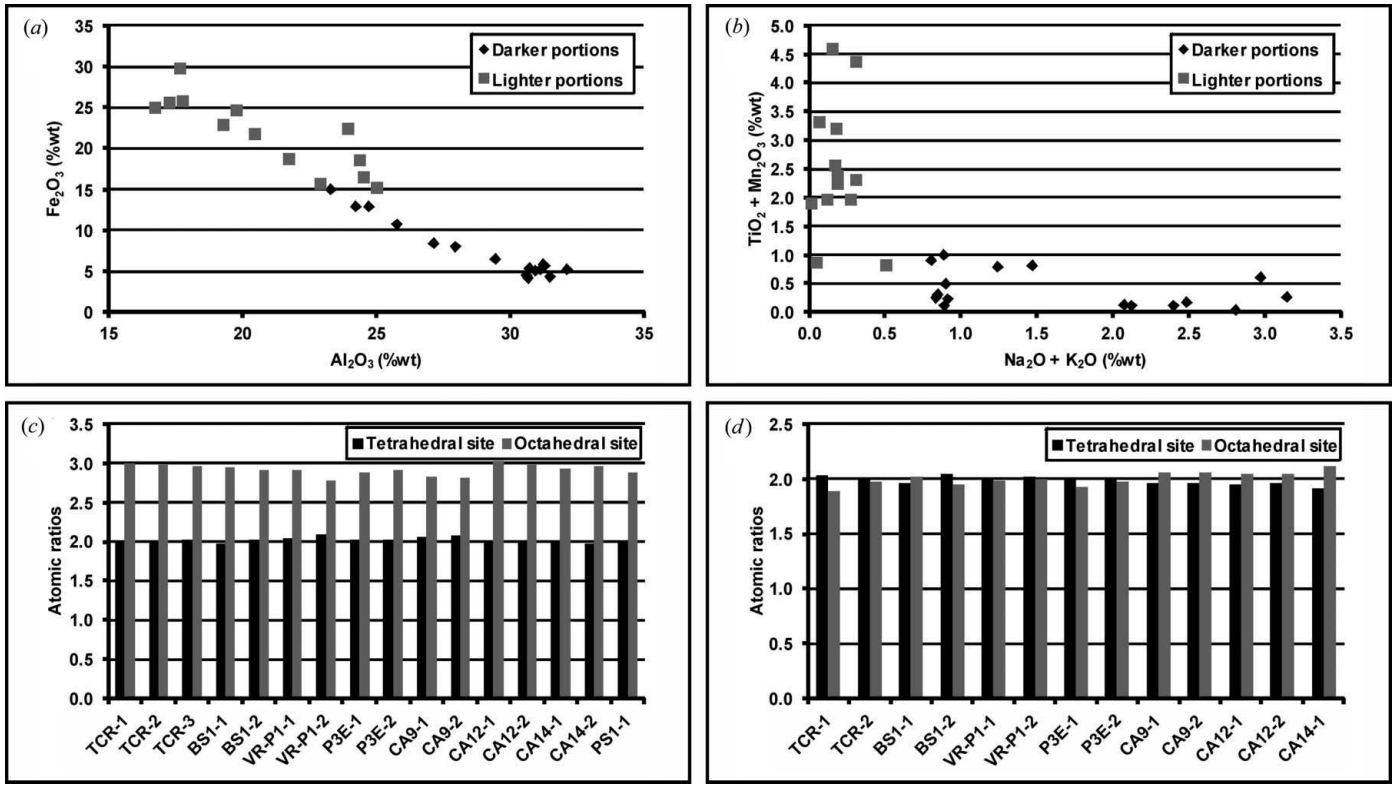

Figure 7
EMP-WDS analyses on the skeletal structures of the analysed clinker relicts. (*a*) Al_2O_3 *versus* Fe_2O_3 scatter plot. (*b*) $Na_2O + K_2O$ *versus* $TiO_2 + Mn_2O_3$ scatter plot. (*c*) Darker portions: sum of the calculated atomic ratios partitioned between tetrahedral and octahedral sites of an aluminate structure, as suggested by Taylor (1997). (*d*) Lighter portions: sum of the calculated atomic ratios partitioned between tetrahedral and octahedral sites of a ferrite structure, as suggested by Taylor (1997).

tion in the analysed relicts, with a pseudomorphic substitution of hydration products after alite and belite.

3.3. EBSD

Several EBSD analyses were performed in the same areas of the clinker relicts analysed by EMP-WDS. Typical EBSPs, acquired from four representative samples (BS1, P3E, CA12 and CA14), are reported in Figs. 8 and 9.

The EBSD analysis of cementitious materials is technically rather difficult, because of the complex nature of such polygranular and polyphasic materials and the occurrence of marked surface effects, which are inconvenient for EBSD purposes. However, accurate measurements allowed us to obtain interpretable EBSPs from most of the point analyses performed on the phases in the skeletal portions of the relicts and to identify their crystalline nature. The solid constituents of the portions enclosed in the grains never produced measurable diffraction signals, confirming their highly disordered or amorphous nature.

Concerning the phase identification, the iron-rich portions characterized by a strong BSE signal always yield sharp patterns univocally indexed as ferrite (Fig. 8), with mean

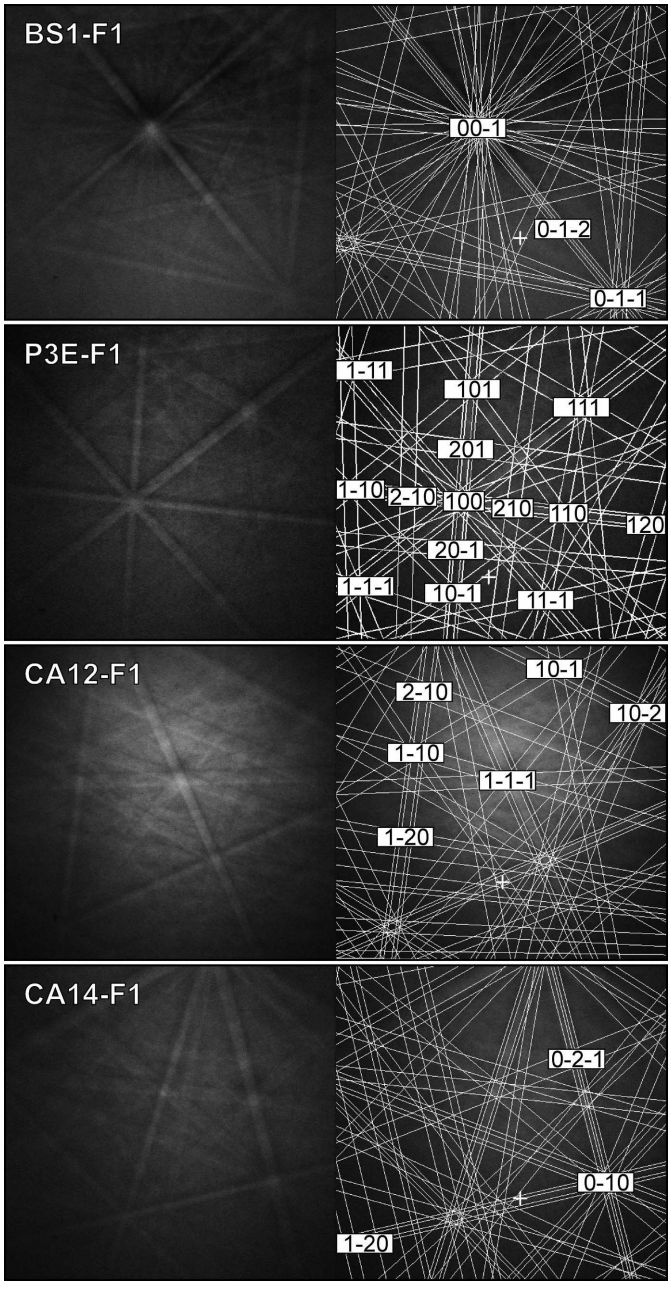

Figure 8
Raw and indexed representative EBSPs of ferrite phases from four different samples. The points of analysis are circled in the previous figures, and the relative EMP-WDS analyses are reported in Table S2.

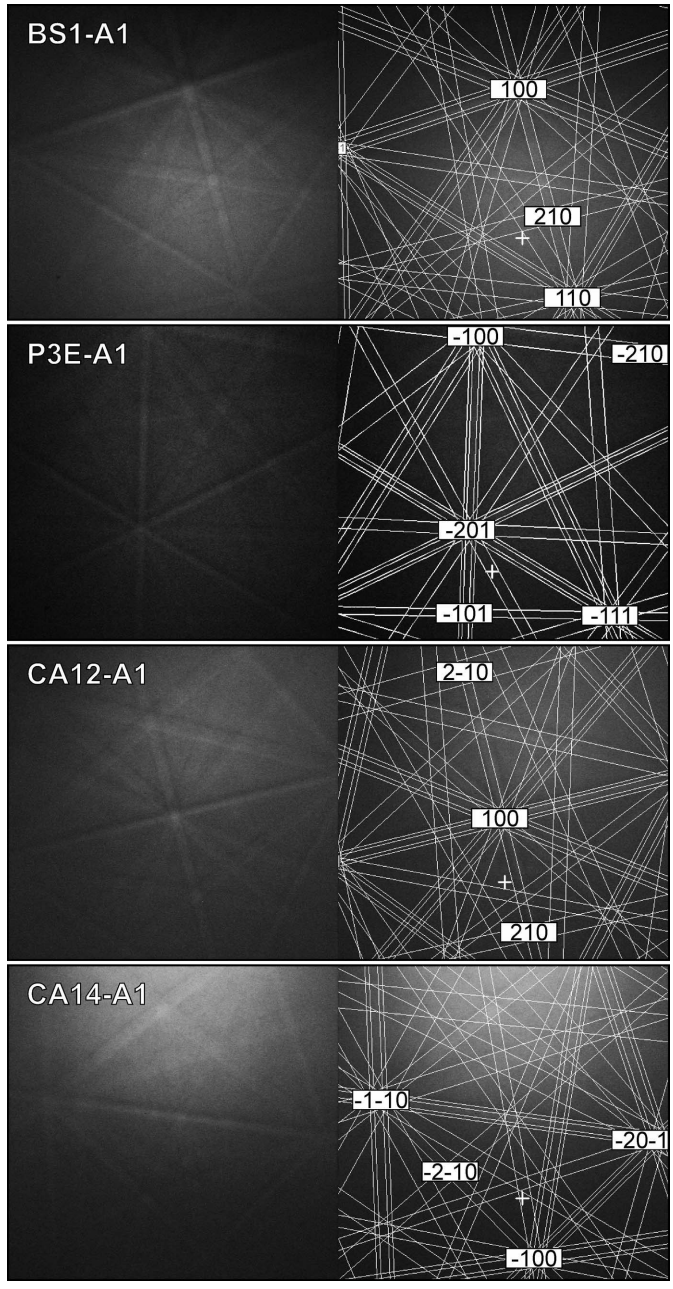

Figure 9
Raw and indexed representative EBSD patterns of aluminate phases from four different samples. The points of analysis are circled in the previous figures, and the relative EMP-WDS analyses are reported in Table S1.

angular deviation (MAD) values always below 1. A common feature observed through EBSD analysis in the majority of the analysed relicts is the tendency of ferrite to grow forming aggregates of crystals showing no preferred orientations, as indicated by the different EBSPs obtained on adjacent spot analyses within the same area.

EBSPs obtained from the aluminium-rich portions generally have a lower diffraction signal intensity (Fig. 9). They can be systematically indexed with the structures of aluminate with MAD values below 1, although it is hard to distinguish between the orthorhombic and the cubic cells owing to the strong similarity in the lattice parameters of the two polymorphs and related pseudosymmetry problems, which may heavily affect EBSD analyses (Wright & Nowell, 2006). Multiple EBSPs acquired in the same area of the skeleton commonly yield nearly the same crystallographic orientation, indicating the tendency of the phase to form relatively large single crystals.

The features observed by point EBSD analyses have been confirmed by simultaneous EDS-EBSD mapping on selected test samples. The results on a representative clinker relict in the CA12 sample are reported in Fig. 10. The secondary electron image acquired at 70° stage tilting (Fig. 10*a*) clearly shows the issues related to the difficulties in preparing such materials: even after accurate polishing procedures, the sample surface is still characterized by a marked roughness, which causes charging, drift and shadowing phenomena. Despite these problems, the simultaneous mapping was successful. EDS maps powerfully discriminate between iron-rich ferrite portions and aluminium-rich aluminate portions (Fig. 10*b*), and it is possible to observe a perfect correspondence of the chemically discriminated regions to those present in the EBSD map (Fig. 10*c*), which are obtained by indexing of the diffraction patterns. The simultaneous analysis is a rigorous confirmation of the crystalline nature of the compounds and the mineralogical discrimination performed separately. In this experiment the subtle discrimination between cubic and orthorhombic aluminate forms was not possible because of the strong pseudosymmetry between the two phases. Finally, the orientation map (Fig. 10*d*) also confirmed the overall aptitude of ferrite to grow forming a polycrystalline non-oriented microstructure, while aluminate, showing preferred orientation, tends to develop preferentially as an individual crystal.

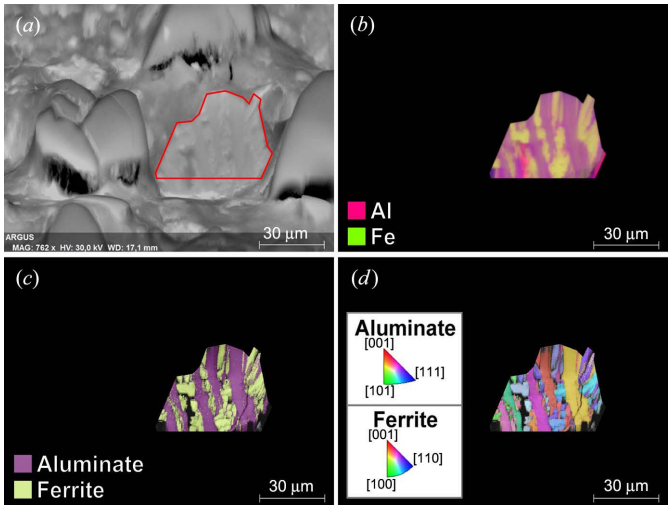

Figure 10
Simultaneous EDS-EBSD mapping on a clinker relict within the CA9 sample. (*a*) Secondary electron image of the relict, acquired at 70° stage tilting (analysed area marked in red). (*b*) EDS composite chemical map, obtained by merging aluminium (in magenta) and iron (in green) elemental maps (*c*) EBSD phase map: aluminate in purple, ferrite in green–yellow. (*d*) Inverse pole figure (IPF) orientation map (IPF colour schemes are reported in the box).

Although the chemical data already indicated the presence of the interstitial phase in the anhydrous state, only the complete micromineralogical analyses based on the crystallography of the clinker phases have proven univocally their nature, excluding any possible substitution of hydrated phases after aluminate and ferrite.

4. Discussion and conclusions

In the present study, a multi-analytical characterization strategy was applied to the binder residuals of several aged cementitious materials, selected because of their diverse typology, composition, age of manufacturing and conservation state. Thanks to the innovative combined approach of microstructural analysis by SEM-EDS, quantitative chemical microanalysis by EMP-WDS and microcrystallographic analysis by EBSD, for the first time extensively applied in the field of cementitious materials science, several key results can be outlined:

(i) Complex cementitious materials cannot be considered fully hydrated even over aging periods of years and even in open systems subjected to intense percolation of water. Measurable amounts of partially or totally non-reacted clinker phases are invariably observable.

(ii) Clinker relicts never show total passivation; rather, a degree of selective reaction of some mineral constituents is common. Specifically, calcium silicates in the clinker grains are always highly or totally hydrated, while the interstitial aluminate/ferrite phase constituents within the analysed clinker relicts are characterized by a substantial permanence at the anhydrous state.

(iii) The selective reaction of specific phase constituents in the relict clinker grains directly affects their microstructure, causing the permanence of peculiar skeletal structures of mainly non-reacted interstitial phase. Aluminate and ferrite crystallize in some cases in large and well separated microstructural domains, while in other cases a more random intergrowth of the phases is observable. The interstitial phase encloses and surrounds the grains of the former anhydrous calcium silicates, which retain the crystalline shape of the original constituents, but they are for the most part filled by hydration products.

(iv) Aluminate and ferrite are never chemically pure, being always characterized by marked isomorphic and polymorphic chemical substitutions. In more detail, aluminates are invariably composed of relevant amounts of iron and alkalis, while

ferrites are characterized by the presence of substituting titanium and manganese, plus silicon and magnesium. Stoichiometric recalculation indicates that these phases are often loaded by vacancy defects.

(v) Aluminate and ferrite are always well crystallized, as demonstrated by the fact that the EBSD technique provides clear and characteristic diffraction patterns. Identification of the aluminate polymorphs by EBSD alone is usually prevented by the intrinsic limitations of the technique, so a tentative differentiation between the orthorhombic and cubic structures can only be achieved by cross checking micromineralogical and microchemical data. As regards the crystalline fabrics, aluminate has the tendency to form single crystals inside each single microstructural domain, while ferrite forms aggregates of crystals with nearly random orientations.

(vi) The ubiquitous reaction of calcium silicates into hydrous poorly crystalline or amorphous phases is confirmed by both chemical and mineralogical data.

Taking into account the obtained results in the perspective of the reaction mechanisms of cementitious materials, several considerations can be put forward.

First of all, the occurrence of relict clinker particles with dimensions always higher than 20 μm is consistent with the theory defined by the Parrot and Killoh empirical equation (Parrot & Killoh, 1984). This function expresses a lowering of the reaction rate as the degree of reaction increases, related to a high degree of reaction of smaller binder fractions during the first phases of hydration (acceleration and first deceleration period) owing to the higher exposed reactive surface, with a subsequent slow down of the reaction involving the coarser particles due to both the reduction in the surface area of the reactive phase and the space filling controlling mechanisms associated with the growth of hydrated phases (Scrivener & Nonat, 2011).

On the other hand, the progression of a selective reaction process of calcium silicates in the larger grains clearly excludes the possibility of total passivation of the particles, because of a diffusion controlling mechanism related to the formation of an external, low permeability layer of hydrated phases. Furthermore, this feature is apparently at odds with ample theoretical and experimental evidence indicating the interstitial phase constituents, in particular aluminate, as the most reactive components in cementitious systems. Several factors may be invoked to explain this paradoxical evidence. A possible mechanism considered in the literature for both aluminate and ferrite phases (Boikova, 1986) is the formation of a passivating layer of iron-rich reaction products over the exposed surfaces of the aluminate-rich interstitial phase in the later stages of reaction, with consequent slowdown and cessation of the hydration process. The present study found no evidence of such layers in the investigated samples. Another factor that should be considered is the modified reactivity of the clinker phases (and specifically of aluminate) under the influence of substituting ions, which is particularly relevant in materials of industrial production, as shown by the presented analyses. The influence of foreign ions in the cement system can condition the microstructural and chemical properties of the materials, including the dissolution reaction of the interstitial phases, both because of structural substitutions and because of the occurrence of foreign ions in solution. Regarding this topic, the influence of transition metals like chromium and zinc in the variation of hydration kinetics of clinker phases is well known in the literature (Boikova, 1986; Taylor, 1997), mainly because of the increase of crystal defects related to the introduction of these elements in the crystal structure of the phases. For the same reason, apart from the hypothesis of passivation layer formation, the reaction of interstitial phase constituents is delayed by increasing amounts of iron in the crystal structures (Boikova *et al.*, 1977). Furthermore, the influence of alkali metal ions on the reduction of the reactivity of aluminate is widely known (Boikova *et al.*, 1977; Spierings & Stein, 1976; Taylor, 1997). This feature may be related to structural differences, but considering that the reaction of pure C_3A is delayed by addition of NaOH in solution, the influence of ion concentrations in solution may not be negligible. Of course, a number of other more complex solutions could be invoked, such as the inhibiting power of sulfate ions acting as passivating agents for the dissolution of aluminate, probably due to preferential adsorption at defect sites and consequent inhibition of etch pit formation (Bullard *et al.*, 2011).

It is not the aim of this work to identify all the possible mechanisms acting during the long period of hydration of real cementitious systems. However, at this stage it is important to pinpoint that these processes, if influential in simplified systems, are to be considered dramatically exacerbated in real systems, with several mineralogical phases belonging to the aggregate fraction and subjected to possible dissolution processes in an alkaline environment, thus justifying possible inertization phenomena of phases normally considered fully soluble. From this perspective, a reliable prediction of the long-term behaviour and durability of such materials cannot exclude a careful investigation of the hydration kinetics well beyond the generally considered maturation period.

Support by Mapei S.p.A. in the framework of the Mapei-UNIPD research agreement is acknowledged. The technical staff at the Department of Geosciences of the University of Padua and at the Institute of Geosciences and Georesources of the National Research Council (IGG-CNR) are thanked for analytical support. In particular, Leonardo Tauro and Raul Carampin kindly helped in the sample preparation procedures and electron microprobe analyses, respectively. The simultaneous EDS-EBSD experimental sessions were supported by Bruker Nano GmbH, whose contribution to this project is greatly appreciated. Finally, Francesca Andolfo is gratefully acknowledged for revising the English text.

References

Adams, B. L., Wright, S. I. & Kunze, K. (1993). *Metall. Trans. A*, **24**, 819–831.

Asaga, K., Ishizaki, M., Takahashi, S., Konishl, K., Tsurumi, T. & Daimon, M. (1992). *Proceedings of the 9th International Congress on the Chemistry of Cement*, pp. 181–187. New Delhi: National Council for Cement and Building Materials.
Bishnoi, S. & Scrivener, K. L. (2009). *Cement Concrete Res.* **39**, 266–274.
Boikova, A. I. (1986). *Proceedings of the 8th International Congress on the Chemistry of Cement*, pp. 19–33. Rio de Janeiro: Finep.
Boikova, A., Domansky, A., Paramonova, V., Stavitskaja, G. & Nikushchenko, V. (1977). *Cement Concrete Res.* **7**, 483–492.
Boikova, A. I., Esayan, A. & Lazukin, V. (1980). *Proceedings of the 7th International Congress on the Chemistry of Cement*, pp. 183–185. Paris: Editions Septima.
Bullard, J. W. (2008). *J. Am. Ceram. Soc.* **9**, 2088–2097.
Bullard, J. W., Jennings, H. M., Livingston, R. A., Nonat, A., Scherer, G. W., Schweitzer, J. S., Scrivener, K. L. & Thomas, J. J. (2011). *Cement Concrete Res.* **41**, 1208–1223.
Colville, A. A. & Geller, S. (1972). *Acta Cryst.* B**28**, 3196–3200.
Costoya, M. M. (2008). PhD thesis, École Polytechnique Fédérale de Lausanne, Switzerland.
Favero, M. (2013). PhD thesis, University of Padua, Italy.
Gaidis, J. M. & Gartner, E. M. (1989). *Materials Science of Concrete*, Vol. 2, edited by J. Skalny & S. Mindess, pp. 9–39. Westerville: American Ceramic Society.
Gao, X., Lo, Y., Tam, C. & Chung, C. (1999). *Cement Concrete Res.* **29**, 805–812.
Garrault, S., Nicoleau, L. & Nonat, A. (2010). *Proceedings of CONMOD*, pp. 91–94. École Polytechnique Fédérale de Lausanne.
Garrault, S. & Nonat, A. (2001). *Langmuir*, **17**, 8131–8138.
Gartner, E. M. & Gaidis, J. M. (1989). *Materials Science of Concrete*, Vol. 1, edited by J. Skalny, pp. 95–125. Westerville: American Ceramic Society.
Gartner, E. M., Young, J. F., Damidot, D. A. & Jawed, I. (2002). *Structure and Performance of Cements*, 2nd ed., edited by J. Bensted & P. Barnes, pp. 57–113. New York: Spon Press.
Gebauer, J. & Harnik, A. (1975). *Cement Concrete Res.* **5**, 163–169.
Ghose, A. & Barnes, P. (1979). *Cement Concrete Res.* **9**, 747–755.
Goldstein, J. I., Romig, A. D. Jr, Newbury, D. E., Lyman, C. E., Echlin, P., Fiori, C., Joy, D. C. & Lifshin, E. (1992). *Scanning Electron Microscopy and X-ray Microanalysis: A Text for Biologists, Materials Scientists, and Geologists*. New York: Springer.
Gutteridge, W. A. & Dalziel, J. A. (1990). *Cement Concrete Res.* **20**, 778–782.
Harrisson, A., Taylor, H. & Winter, N. (1985). *Cement Concrete Res.* **15**, 775–780.
Hearn, N., Detwiler, R. J. & Sframeli, C. (1994). *Cement Concrete Res.* **24**, 633–640.
Hoshino, S., Yamada, K. & Hirao, H. (2006). *J. Adv. Concr. Technol.* **4**, 357–367.
Juilland, P., Gallucci, E., Flatt, R. & Scrivener, K. (2010). *Cement Concrete Res.* **40**, 831–844.
Kocaba, V. (2010). PhD thesis, École Polytechnique Fédérale de Lausanne, Switzerland.
Kristmann, M. (1978). *Cement Concrete Res.* **8**, 93–102.
Lloyd, G. E. (1987). *Mineral. Mag.* **51**, 3–19.
Lothenbach, B. & Winnefeld, F. (2006). *Cement Concrete Res.* **36**, 209–226.
Merlini, M., Artioli, G., Cerulli, T., Cella, F. & Bravo, A. (2008). *Cement Concrete Res.* **38**, 477–486.
Mumme, W. G., Hill, R. J., Bushnell-Wye, G. & Segnit, E. R. (1995). *Neues. Mineral.* **169**, 35–68.
Nishi, F. & Takéuchi, Y. (1975). *Acta Cryst.* B**31**, 1169–1173.
Nishi, F., Takéuchi, Y. & Maki, I. (1985). *Z. Kristallogr.* **172**, 297–314.
Parrot, L. J. & Killoh, D. C. (1984). *Proc. Br. Ceram. Soc.* **35**, 41–54.
Peruzzo, L., Fenzi, F. & Vigato, P. A. (2011). *Archaeometry*, **53**, 178–193.
Pouchou, J. L. & Pichoir, F. (1985). *Microbeam Analysis Proceedings*, edited by J. T. Armstrong, pp. 104–106. San Francisco Press.
Prior, D. J., Boyle, A. P., Brenker, F., Cheadle, M. C., Day, A., Lopez, G., Peruzzo, L., Reddy, S., Spiess, R., Timms, N. E., Trimby, P., Wheeler, J. & Zetterström, L. (1999). *Am. Mineral.* **84**, 1741–1759.
Quennoz, A. & Scrivener, K. L. (2012). *Cement Concrete Res.* **42**, 1032–1041.
Sarkar, S. L. & Roy, D. M. (1984). *Proceedings of the 6th International Conference on Cement Microscopy*, pp. 37–46. Albuquerque: International Cement Microscopy Association.
Schlegel, M., Sarfraz, A., Müller, U., Panne, U. & Emmerling, F. (2012). *Angew. Chem.* **51**, 4993–4996.
Schwartz, A. J., Kumar, M., Adams, B. L. & Field, D. P. (2009). *Electron Backscatter Diffraction in Materials Science*, 2nd ed. Berlin: Springer.
Scrivener, K. L. (2004). *Cement Concrete Comput.* **26**, 935–945.
Scrivener, K. L. & Nonat, A. (2011). *Cement Concrete Res.* **41**, 651–665.
Secco, M. (2012). PhD thesis, University of Padua, Italy.
Spierings, G. & Stein, H. (1976). *Cement Concrete Res.* **6**, 265–272.
St John, D. A., Poole, A. B. & Sims, I. (1998). *Concrete Petrography, A Handbook of Investigative Techniques.* London: Arnold Publishing.
Takéuchi, Y., Nishi, F. & Maki, I. (1980). *Z. Kristallogr.* **152**, 259–307.
Taylor, H. F. W. (1997). *Cement Chemistry.* New York: Thomas Telford Publishing.
Taylor, H. F. W., Barret, P., Brown, P. W., Double, D. D., Frohnsdorff, G., Johansen, V., Ménétrier-Sorrentino, D., Odler, I., Parrott, L. J., Pommersheim, J. M., Regourd, M. & Young, J. F. (1984). *Mater. Struct.* **17**, 457–468.
Taylor, R., Richardson, I. & Brydson, R. (2010). *Cement Concrete Res.* **40**, 971–983.
Viani, A., Gualtieri, A. F., Secco, M., Peruzzo, L., Artioli, G. & Cruciani, G. (2013). *Am. Mineral.* **98**, 1095–1105.
Wilkinson, A. J. & Hirsch, P. B. (1997). *Micron*, **28**, 279–308.
Wong-Ng, W., McMurdie, H., Paretzkin, B., Hubbard, B. & Dragoo, A. (1987). *Powder Diffr.* **2**, 195–202.
Wright, S. I. & Nowell, M. M. (2006). *Microsc. Microanal.* **12**, 72–84.